Extreme Monolayer-Selectivity of Hydrogen-Plasma Reactions with Graphene

Georgi Diankov,[†,‡,¶] Michael Neumann,[†,¶] and David Goldhaber-Gordon[†,*]

[†]Department of Physics and [‡]Department of Chemistry, Stanford University, Stanford, California, United States. [¶]These authors contributed equally to this work.

ABSTRACT We study the effect of remote hydrogen plasma on graphene deposited on SiO_2. We observe strong monolayer selectivity for reactions with plasma species, characterized by isotropic hole formation in the basal plane of monolayers and etching from the sheet edges. The areal density of etch pits on monolayers is 2 orders of magnitude higher than on bilayers or thicker sheets. For bilayer or thicker sheets, the etch pit morphology is also quite different: hexagonal etch pits of uniform size, indicating that etching is highly anisotropic and proceeds from pre-existing defects rather than nucleating continuously as on monolayers. The etch rate displays a pronounced dependence on sample temperature for monolayer and multilayer graphene alike: very slow at room temperature, peaking at 400 °C and suppressed entirely at 700 °C. Applying the same hydrogen plasma treatment to graphene deposited on the much smoother substrate mica leads to very similar phenomenology as on the rougher SiO_2, suggesting that a factor other than substrate roughness controls the reactivity of monolayer graphene with hydrogen plasma species.

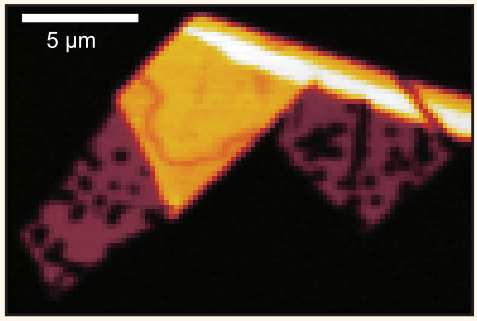

KEYWORDS: graphene · chemical reactivity · hydrogen plasma · preferential etching

Graphene is a two-dimensional honeycomb lattice of sp^2-bonded carbon atoms, renowned for its exceptional electronic, mechanical, and optical properties.[1−3] The desire to exploit the unusual properties of graphene in technological applications has led to intense efforts to tailor its properties by chemical modification and functionalization, with a view to opening a band gap,[4,5] charge-transfer doping,[6,7] interfacing graphene with other materials[8] and modifying graphene's optical properties.[9] Understanding the chemical reactivity of graphene is of fundamental importance to the rational use of this material in electrochemical devices,[10] biosensing,[11] biocompatible materials,[12] and for energy harvesting.[13] Intriguingly, several groups have observed anomalously high reactivity of single-layer graphene in reactions with diazonium salts,[14,15] in electrochemical redox reactions,[16] and in reactions with atomic hydrogen generated by the dissociation of a hydrogen silsesquioxane film.[17] A full understanding of the factors behind monolayer graphene chemistry, however, remains elusive.

One promising approach to modifying the chemical and physical properties of graphene is treatment with gases or plasma at elevated temperatures. High-temperature annealing in the presence of oxygen has been found to induce both strong p-type doping[18] and formation of etch pits in monolayer graphene.[19] Inspired by the rich interactions of carbon nanotubes with ionized discharges, researchers have also used plasma to chemically modify graphene.[20,21] Hydrogen plasma has emerged as a particularly attractive tool for chemical modification of graphene and opening of a band gap for various applications. At present, key aspects of the reactions between graphene and hydrogen plasma are little-understood. For instance: Why are monolayers more reactive than thicker sheets toward hydrogenation in some experimental configurations?[22] Can plasma treatment produce well-defined edge structures in graphene, while leaving the basal plane pristine? Elucidating these key issues could enable fabrication of advanced graphene nanoribbon devices that overcome the limitations of lithographically etched nanoribbons: transport dominated

* Address correspondence to goldhaber-gordon@stanford.edu.

Received for review October 23, 2012 and accepted January 17, 2013.

Published online January 17, 2013
10.1021/nn304903m

by disorder from a rough potential landscape in the interior of the ribbons and likely also from ragged edges.[23,24] Besides a confinement-driven bandgap, perfect hydrogen-terminated graphene nanoribbons have been predicted to exhibit more exotic phenomena, such as spin-valve behavior.[25]

Treatment of graphene with a remote DC plasma mixture of hydrogen and argon was first reported to lead to slow, reversible hydrogenation, preferential for monolayers and conjectured to result from the chemisorption of hydrogen radicals.[22] Conversely, when graphene is directly immersed in an RF plasma discharge, fast hydrogenation preferential for bilayers and thicker sheets, rather than monolayers, has been observed and argued to result from chemistry with energetic hydrogen ions.[26] The chemical reactivity of graphene toward hydrogen plasma species has also been used to pattern graphene. Using RF hydrogen plasma treatment, anisotropic etching along well-defined crystallographic directions in single- and multilayer graphene sheets was recently reported.[27,28] In combination with lithographic patterning, hydrogen plasma etching was used to produce graphene nanoconstrictions. Intrigued by the possibilities present in these approaches, we have investigated the interactions of graphene with hydrogen plasma to better understand and, in the future, control the chemical reactivity of graphene.

RESULTS/DISCUSSION

We prepare monolayer and multilayer graphene samples by micromechanical cleavage from highly oriented pyrolytic graphite (HOPG) and deposit them on oxidized silicon substrates.[29] Samples of graphene on SiO_2 are exposed to remote hydrogen plasma inside a tube furnace at controlled temperature, at a hydrogen pressure of ~0.4 Torr.

Reaction with hydrogen plasma species results in strikingly different phenomena on monolayer graphene sheets as compared to bilayer and thicker sheets. Tapping mode AFM images of samples processed for 10 min at a temperature of 500 °C (Figure 1a–c) show that on monolayer graphene, numerous circular etch pits are formed, in addition to etching from the sheet edges. In contrast, very little etching is observed on multilayer sheets. The incidence rate of etch pits in bilayer and thicker sheets (discussed in more detail below) is approximately 2 orders of magnitude lower than that of

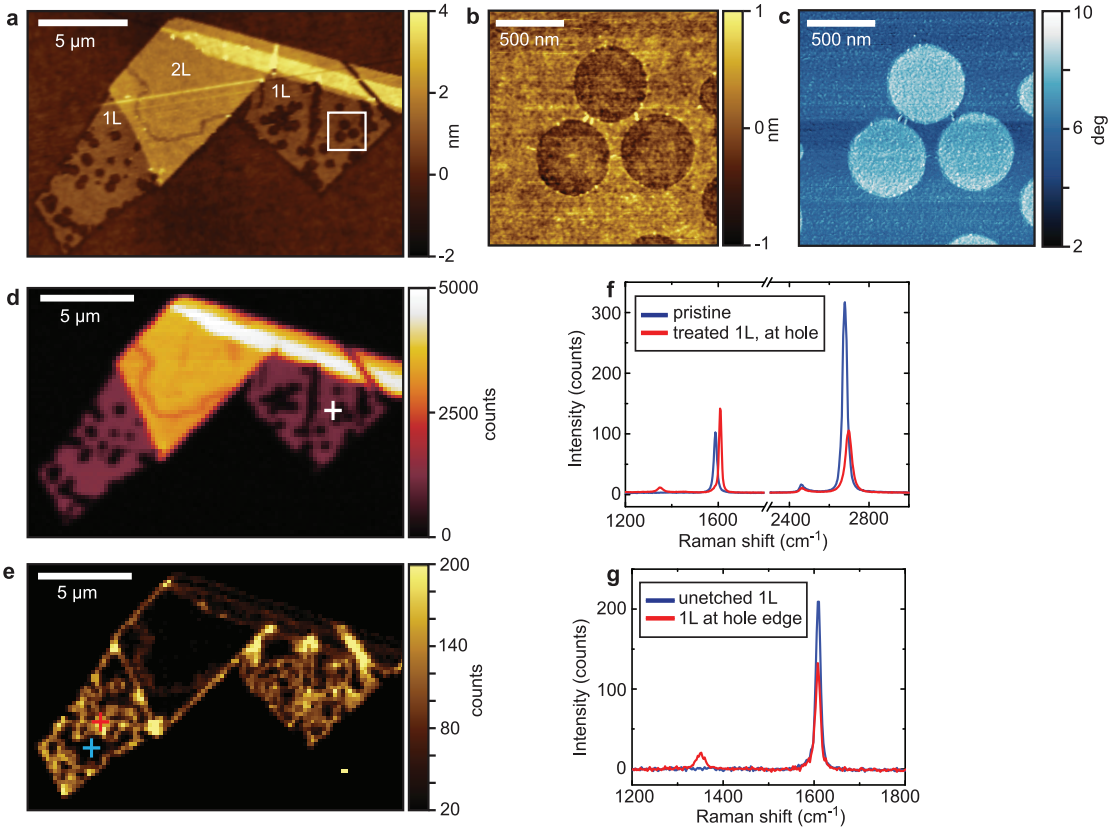

Figure 1. Effect of hydrogen plasma treatment at 500 °C for 10 min. (a) Tapping mode AFM topography image of monolayer and multilayer graphene deposited on SiO_2. Reactions are highly selective for monolayer sheets, where isotropic etching takes place. Occasional formation of etched trenches is visible in thicker sheets. (b) AFM topography and (c) phase shift images of area marked in panel a, showing circular etch pits. (d) Raman G-band and (e) D-band mapping of the sample shown in panel a. A high D-band intensity is found exclusively at the sheet edges and at the boundaries of etch pits. (f) Raman spectra acquired on monolayer graphene, before and after plasma treatment, at the spot marked with a white cross in panel d. (g) Raman spectra acquired close to an etch pit (red line) and away from etch pits (blue line), at the locations indicated in panel e.

circular pits in monolayer graphene, reflecting the very high monolayer selectivity of the reaction with hydrogen plasma.

Raman spectra (Figure 1d−g) provide complementary information. The intensity of the Raman D-band, taken as a measure of the presence of defect sites in the graphene lattice,[30] is enhanced only at edges of sheets, and in the immediate vicinity of etch pits in monolayer graphene, whereas it is absent elsewhere on monolayer sheets, and in the basal plane of multilayer sheets. We interpret these observations as indications that hydrogen plasma species react preferentially with monolayer graphene, and the resulting formation of volatile products leads to removal of carbon atoms. Additionally, the spatial pattern of enhanced D-band intensity (Figure 1e) shows that no hydrogenation takes place in the unetched basal plane of monolayer graphene.

Both etch processes in monolayer graphene—etching from the edges and formation of circular etch pits in the basal plane—are isotropic. Figure 2 shows the temperature dependence of etch rates in monolayer graphene, at the sheet edges (red triangles) and in round etch pits (red circles), as determined from AFM images. For etch pits, we extract etch rates from the size of the largest circular hole in a given sample, since the spread in hole size reflects the spread in etch pit nucleation time (discussed below). Etching proceeds fastest around 400 °C, at a rate of approximately 40 nm/min, whereas no etching is observed at 700 °C, and very low

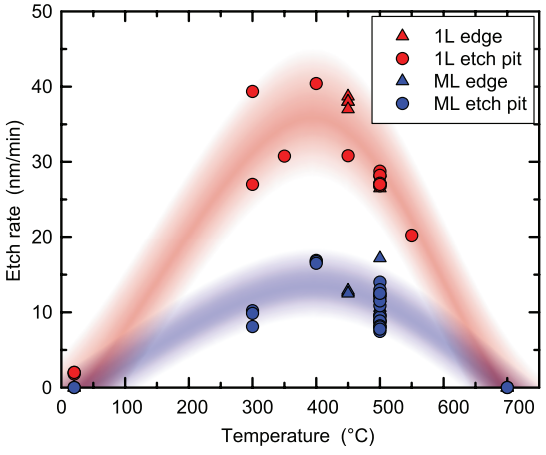

Figure 2. Dependence of etch rate on furnace temperature, for 10 min of hydrogen plasma exposure. The etch rate is calculated as half the etch pit diameter divided by treatment duration. For monolayer (1L) graphene, uniform etching from the sheet edges (red triangles) and circular etch pit formation within the basal plane (red circles) proceed at very similar rates, suggesting that the same isotropic etch mechanism controls both processes. For circular etch pits, only the diameter of the largest hole found in each sample is shown. For multilayer (ML) graphene, uniform etching from the sheet edges (blue triangles) occurs alongside anisotropic etching in the basal plane (blue circles). The diameter of hexagonal etch pits is taken as the distance between opposing sides. All etch pit dimensions are determined from AFM images. Red and blue swathes are guides to the eye.

etch rates ≤2 nm/min are seen at room temperature. Etching of circular pits and from monolayer edges occur at comparable rates, indicating that these two phenomena are manifestations of the same reaction process.

We have observed that during hydrogen plasma processing of our samples, the placement of the sample chip relative to its quartz "tube boat" carrier can influence the monolayer graphene etch rate; moving the chip closer to the end of the boat nearer the glow discharge by ∼10 mm causes an etch rate enhancement sufficient to remove all monolayer sheets within 10 min. We have not explored this phenomenon further so far, and our discussion does not cover the small set of samples (6 samples out of a total 45) on which monolayer graphene sheets were removed entirely. On all other samples, our observations are both qualitatively and quantitatively reproducible, which suggests that the two sets of samples correspond to two different plasma regimes, and we believe that restricting our discussion in this way does not introduce a bias in our results.

We now discuss a number of observations that allow us to speculate on the reaction mechanism between monolayer graphene and hydrogen plasma species. First, we observe that isotropic etching proceeds from all edges of monolayer graphene sheets, including both free sheet edges and the edges of the newly formed circular etch pits. Edge sites are known to be more reactive than regular sites within the sp^2-bonded lattice,[14] and the above observation suggests that the presence of reactive sites within the graphene monolayer is necessary for etching to progress. In contrast, no comparable etching of monolayer sheets proceeds from the boundaries between monolayer and multilayer sheets.

Second, while the rate of etching from monolayer edges seems identical on all sides of the sheet (see Figure 3), AFM and Raman scans show that etch pits within the basal plane of monolayer sheets have a wide distribution of diameters (see Figures 1 and 3), with the largest radii comparable to etching from the edges. Under the assumption that the two etch processes share a common mechanism and proceed at the same rate, this size distribution indicates that etch pits do not originate from preexisting lattice defects, but instead nucleate continuously throughout the duration of hydrogen plasma exposure.

Third, a large portion of our AFM scans exhibit a clear contrast between a "pristine" SiO_2 substrate located away from graphene sheets, and a "reacted" substrate that was formerly covered by monolayer graphene but is exposed after graphene removal during hydrogen plasma treatment, leaving an imprint of the original shape of the monolayer sheet (see Figure 3c,d and Supporting Information, Figure S3a,b). In such images, the AFM topography signal exhibits an apparent depression of the reacted substrate by 0.3−0.5 nm with

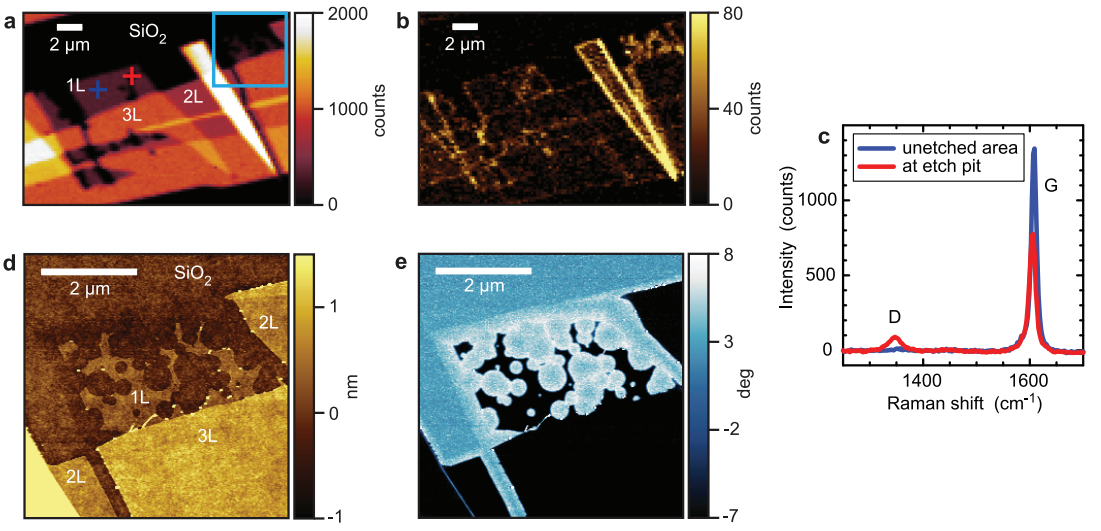

Figure 3. Clustering of etch pits in monolayer graphene, and SiO_2 substrate participation in reaction between graphene and hydrogen plasma, for a sample exposed to hydrogen plasma at 450 °C for 10 min. (a) Raman G-band and (b) D-band mapping, showing an inhomogeneous spatial distribution of basal plane etch pits in monolayer graphene. The blue square, containing a mostly etched monolayer sheet, marks the area of the AFM scan shown in panels d and e. (c) Raman spectra on monolayer graphene, close to an etch pit (red line) and away from etch pits (blue line), at the locations indicated by crosses in (a). (d) AFM topography and (e) phase shift images. Where monolayer or multilayer graphene has been etched away, an apparent depression of about 0.5 nm is visible in the topography image, and these "reacted" substrate areas exhibit a phase contrast with respect to the "pristine" substrate.

respect to pristine SiO_2, and the cantilever phase lag differs by 1−5° between the two surfaces. This observation suggests that the SiO_2 substrate is not merely an inert support, but participates actively in the reaction of monolayer graphene with hydrogen plasma species. A similar formation of depressions in SiO_2 has been observed after the annealing of defect-seeded monolayer graphene in inert atmosphere.[31]

Fourth, the circular etch pits formed during hydrogen plasma exposure are not always homogeneously distributed across monolayer sheets. Raman and AFM scans of monolayer graphene sheets shown in Figure 3 panels a and c, respectively, illustrate this effect, with etch pits clustered in some areas of monolayer sheets, while other areas are free from etch pits. However, we have not found a clear correlation of the locations of etch pit clusters with sample geometry, such as the distance to neighboring multilayer sheets or to bare substrate areas.

The effect of hydrogen plasma on multilayer graphene sheets is strikingly different from that on monolayers. Etch pits found in multilayer graphene are not only much rarer than in monolayer graphene, but they also have a hexagonal instead of circular shape, both for few-layer sheets (Figure 4a,b) and HOPG plates (Figure 4c). When multiple hexagonal holes are present in the same multilayer graphene sheet, they often appear oriented along the same direction. We take the etch pit orientation and 6-fold symmetry as evidence that the etching of multilayer sheets induced by hydrogen plasma is highly anisotropic and propagates along a preferred crystallographic direction. Moreover, in contrast to the case of monolayer graphene, the hexagonal holes in multilayer graphene are very uniform in size across a particular sample, and in about half of all instances the etch pits are located at step edges. This suggests that etching starts at preexisting lattice defects, and that no further etch pits are nucleated by plasma exposure. The rate at which anisotropic etch pits grow (Figure 2, blue circles) appears to be independent of the thickness of the multilayer sheet, and is approximately by a factor 3 lower than etch rates of monolayer graphene.

The AFM topography and phase contrast between "pristine" and "reacted" SiO_2 substrate discussed above for the case of monolayer graphene is also visible adjacent to multilayer sheets (Figure 3d,e), indicating that uniform etching from the sheet edges occurs also for multilayer graphene. However, the rate of etching from edges in multilayers (Figure 2, blue triangles) is significantly lower than in monolayer graphene.

Occasionally, etched trenches cut through both monolayer and multilayer graphene sheets after hydrogen plasma exposure (for example, see Figures 1a,d,e, and Supporting Information, Figure S2a). The length of such trenches typically spans an entire graphene flake. After a plasma exposure of 10 min, trenches in multilayer graphene have a width of order 300 nm, suggesting a transverse etch rate of 15 nm/min, similar to the etch rates for multilayer graphene shown in Figure 2. We thus speculate that the trenches form by the etching of monolayer and multilayer sheets, originating at preexisting line defects in the graphene lattice, such as grain boundaries.

The isotropic etch process is strictly confined to monolayers: in samples on which a monolayer is in direct

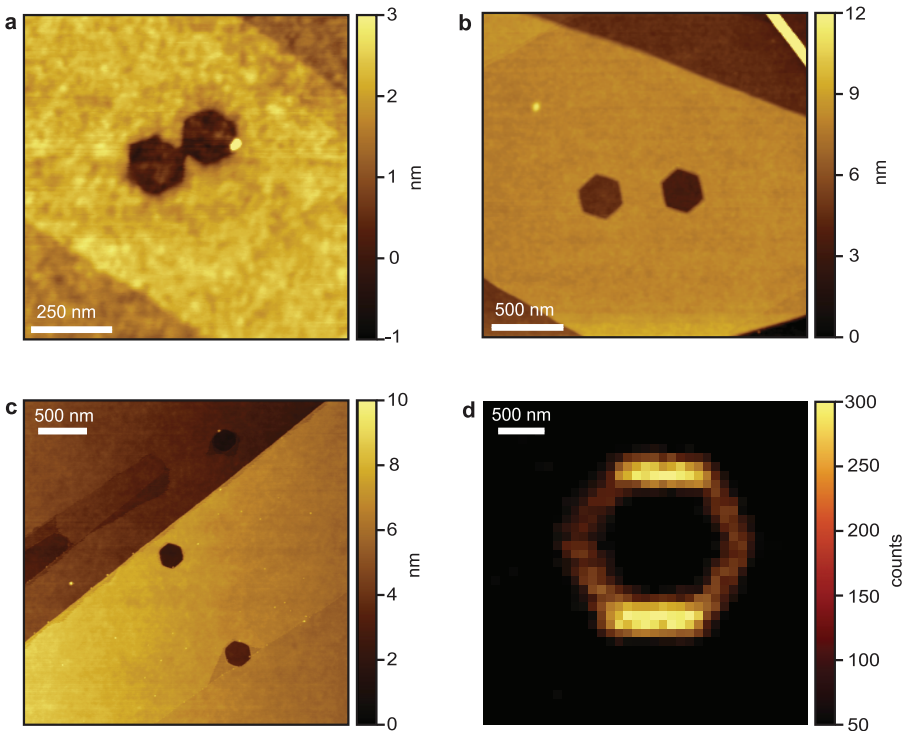

Figure 4. Effect of hydrogen plasma treatment on multilayer graphene and HOPG. (a) Anisotropic etching of a thin graphene sheet (5 layers) after 10 min of hydrogen plasma exposure at 500 °C. (b) Anisotropic etching of thick sheets (>10 layers) after 10 min of hydrogen plasma exposure at 500 °C. (c) HOPG treated at 350 °C. The edges of hexagonal etch pits in images a, b, and c are aligned in parallel, suggesting that etching proceeds preferentially along the same crystallographic axes. An arbitrary offset in the height has been used, as the image did not include bare SiO_2 substrate. (d) Map of the Raman D-band intensity on the edges of a large hexagonal hole formed on HOPG after a 70-min hydrogen plasma treatment at 500 °C. The D-band intensity is negligible away from the hole edges. The intensity is more pronounced on the horizontally aligned edges of the etch pit, as this is the direction of the incoming laser light polarization.

contact with a bilayer, the isotropically formed etch pits terminate at the edge of the bilayer. In contrast, we observe anisotropic, hexagonal etch pit formation exclusively on nonmonolayer sheets, from bilayer graphene to HOPG plates. Our findings are in partial agreement with recent results by other workers,[27,28] who utilized an experimental RF-plasma setup similar to ours. In an initial report of these authors,[27] at a hydrogen pressure of 0.35 Torr (comparable to 0.4 Torr used in our experiment), plasma exposure leads to etch pit formation in monolayer and multilayer graphene, with a temperature-dependent etch rate that is maximal at ~450 °C, and with monolayer sheets being etched 3 times faster than bilayer sheets, all in good agreement with our results. An important difference to our results is that this work[27] does not report a difference in etch pit incidence rate between monolayer and multilayer graphene, whereas we observe an extreme monolayer selectivity. Further, that work reports that anisotropic etching, evidenced by hexagonal holes oriented along the same crystallographic direction, takes place on graphene sheets of all thicknesses, including monolayers,[27] which is in striking contrast to our observation that on monolayer sheets only circular etch pits form. However, in a later publication,[28] the same authors report that anisotropic etch pit formation can be reproduced reliably only for bilayer and thicker sheets, whereas monolayers are not etched anisotropically, and this more recent result is consistent with our findings.

Anisotropic etching on graphite surfaces has been reported in the past. Most commonly, such pits have been seen on graphite heat-treated in oxygen,[32,33] and in reactions with atomic hydrogen.[34] In these studies, etching was proposed to initiate at pre-existing *c*-axis defects, such as screw dislocations. Two of our observations support the view that etching of multilayer graphene and HOPG propagates from pre-existing crystalline defects. First, unlike the etch process in monolayers, thicker sheets and HOPG yield no evidence for continuous nucleation: hexagonal etch pits formed during plasma exposure exhibit a small spread in size at any given temperature, indicating that etching starts at the same time for all etch pits. Moreover, etch pit sizes increase linearly with the duration of plasma exposure, with no apparent increase in etch pit density. HOPG plates treated with hydrogen plasma at 500 °C for 10 min yield etch pits of about 250 nm in size (as defined by the distance between parallel edges of hexagons), with a narrow size distribution, whereas on a sample treated under the same conditions for 70 min all etch pits have sizes of about ~2 μm. The fact that no smaller holes are observed after this longer reaction

time suggests that all etch pits start expanding at the same time, most likely from pre-existing crystal defects, and grow at the same rate. Second, the areal density of holes on thick sheets is significantly lower than that on monolayers, by about 2 orders of magnitude for a treatment duration of 10 min, suggesting that particular sites serve as nucleation centers for multilayer etch pit formation. These characteristics are in marked contrast with the etch process in monolayers, where the size distribution of etch pits is wide, and the areal density of holes is high.

To understand the striking phenomena we observe, it would be helpful to identify the hydrogen plasma species that take part in reactions with graphene samples. Based on prior studies of the parameters of hydrogen discharges at similar pressures and power, we believe that the dominant species in our weakly ionized discharge (ionization rate below 0.1%) are hydrogen radicals (1%) and H^{3+} ions (0.1%), as well as H^{2+} and H^{+} ions (each ~0.0001%).[35] At a distance of 30 cm from the discharge, where our samples are located during treatment, the density of hydrogen radicals is expected to remain almost the same as in the discharge, while that of ions and electrons should be reduced,[36] with H^{3+} ions likely continuing to remain more abundant than other hydrogen ions.[37] Therefore, we are most likely observing the effects of a chemical reaction with hydrogen radicals and H^{3+} ions, similar to the involvement of these species in the temperature-dependent chemical erosion of graphite observed previously.[38−40]

While the mechanisms of etching on monolayers and thicker sheets appear to be different, they are both gasification reactions in which hydrocarbon products, chiefly methane, are formed by reactions with hydrogen radicals and ions. The observation of a reaction rate that exhibits a maximum at a given temperature is typical in reactions between gaseous species and hot solid surfaces, in which volatile products are formed.[41] Previous studies of the reaction between graphite and atomic hydrogen found that the maximum reaction rate occurs between 500 and 600 °C.[41,42] At higher temperatures, the reaction rate decreases sharply due to the thermodynamic instability of methane.[42] While we observe the same type of temperature dependence of the reaction rate, the maximum reaction rate in our experiments occurs at ~400 °C, for both monolayer and multilayer graphene (Figure 2), lower than that seen for graphite in the literature. A possible reason for this behavior is that with increasing temperature, the rate of hydrogen radical recombination into molecules on the hot furnace tube surfaces should rise, leading to a suppression of the hydrogen radical density at the graphene sample[43] and a corresponding decrease in the reaction rate.

While the temperature dependence of the reaction rate can be explained with thermodynamic arguments, a key issue remains regarding the layer-selectivity of the chemical reaction: some parameter must enhance the chemical reactivity of monolayers and lead to continuously nucleating, isotropic etching on monolayers, in contrast to thicker sheets, even bi- and trilayers, in which anisotropic etching at pre-existing point defects occurs. Identifying the parameter responsible for this layer-selective behavior will aid in the understanding of monolayer graphene's chemical properties in general.

Substrate roughness has been invoked as the factor responsible for the enhanced monolayer graphene reactivity.[44] Monolayer graphene conforms with high fidelity to the roughness of the SiO_2 substrate,[45] which leads to some degree of corrugation in the monolayer sheet, and to local breaking of the hexagonal symmetry.[46] Such corrugation might be expected to lead to significant enhancement in the chemical reactivity of monolayers, similar to, though weaker than, the role of curvature in the chemistry of carbon nanotubes.[47]

To test the hypothesis that a much smoother substrate would reduce graphene's reactivity, we performed a control experiment with graphene deposited on cleaved muscovite mica. This atomically smooth substrate has been used to support extremely flat exfoliated graphene monolayers.[48] From AFM scans, the roughness of our as-exfoliated monolayer graphene sheets on mica is 50 ± 15 pm (rms), almost identical to the roughness of the mica substrate. This is several times smaller than the roughness of graphene deposited on SiO_2, 135 ± 25 pm (rms), and of our SiO_2 substrates, 165 ± 25 pm (rms). AFM phase images of a monolayer on mica treated with hydrogen plasma at 500 °C (Supporting Information, Figure S9) show round etch pits. Moreover, such etch pits are only seen in monolayers, mirroring the layer selectivity of the etch process of graphene on SiO_2. This suggests that the reactivity of monolayers may not be induced by substrate curvature, as generally believed. At the same time, we observe the typical presence of water adlayers, trapped between mica and graphene,[49] and visible on AFM images (Figure S9). These water islands may lead to some local curvature in graphene that could be partly responsible for its high reactivity even on this ultraflat substrate.

Rather than substrate flatness, interfacial charge transfer, arising from ionized impurities in the substrate or from substrate polarity, could be responsible for the enhancement of chemical reactivity in monolayer graphene. Similar explanations have recently been advanced for the high reactivity of monolayer graphene observed in studies of oxidative gas-phase reactions[50] and in reactions with diazonium salts.[51] Local potential fluctuations in monolayer graphene[52] caused by ionized impurities have been shown to affect carrier scattering and minimum conductivity in graphene.[53] Local fluctuations in the Fermi level could

lead to enhanced reactivity, as suggested for the reaction between monolayer graphene and diazonium compounds.[14,51] Following this logic, thicker graphene layers would have lower reactivity due to better screening of the ionized impurities. In the case of mica, ionized impurities could also play a key role: mica cleavage occurs along planes lined with submonolayers of potassium ions. While the exact surface reconstruction of cleaved mica surfaces in ambient atmosphere is not fully understood, its significant surface polarity[54] could enhance the reactivity of monolayers toward reactions with hydrogen radicals and ions.

In discussing the possible role of interfacial charge transfer on reactivity, we would like to emphasize that the typically seen strong p-type doping of monolayer graphene after heat treatment is probably unrelated to its high reactivity. *In-situ* Raman spectroscopy studies[18,55] have shown that monolayer sheets remain undoped during thermal treatment: p-type doping occurs only when the samples are exposed to oxygen, water, or ambient air, likely due to charge transfer from graphene toward an environmental oxygen-containing species. We infer that our graphene samples are undoped during hydrogen plasma exposure at elevated temperatures, and that the significant upshifts of the Raman G and 2D-bands observed *ex-situ* after treatment (Supporting Information, Figure S6a), corresponding to high levels of p-type doping, arise only after exposure to ambient air. This is supported by the observation that when graphene samples are exposed to hydrogen plasma at room temperature, without thermal pretreatment, monolayer sheets undergo etching (Supporting Information, Figure S6b–d), while the G and 2D-bands remain unshifted, showing that these monolayers are undoped after exposure to ambient air.

CONCLUSION

We have studied the interaction of remote hydrogen plasma with monolayer and multilayer graphene. We observe extremely high monolayer selectivity toward a hydrocarbon-forming reaction with hydrogen radicals and ions, resulting in random, continuously nucleating isotropic holes. This reaction is entirely suppressed on bilayers and thicker sheets, on which a different phenomenon is seen: crystallographically faceted hexagonal etch pits. Since the same monolayer selectivity also occurs on the atomically smooth mica surface, we suggest that substrate polarity or the presence of charged impurities within the substrate, not the degree of substrate roughness, lead to the high chemical reactivity of monolayer graphene. Further studies are needed to explore the reactivity of graphene on substrates in which the charged impurity density is extremely low, such as boron nitride, on which graphene is undoped and exhibits high carrier mobility.[56]

METHODS

Graphene samples are prepared by micromechanical exfoliation from HOPG (Momentive Performance Materials, grade "ZYA") using wafer processing adhesive tape (Ultron Systems, P/N 1007R), and deposited on silicon wafer pieces (n^{++}-doped with As, resistivity $\leq$ 0.005 Ω cm), with 300 nm dry thermal oxide. No metal alignment markers are used. To reduce hydrocarbon contaminants, the substrate surfaces never come into contact with resist and solvents.

Supporting Information, Figure S1 shows a schematic of our vacuum system for hydrogen plasma processing of graphene samples. Our samples are placed inside a one-inch diameter quartz tube, at the center of a split-hinge tube furnace (Lindberg BlueM). Plasma is generated upstream of the furnace, ~30 cm away from the sample, using a capacitor formed by two parallel plates situated outside the vacuum, on either side of the quartz tube. An RF-current source (Comdel CX600) operating at 13.56 MHz is matched to the capacitor by a matching network (ENI MWD-25LD). Process gas flow rates are controlled upstream by mass flow controllers (MKS 1179A), and the gas pressure is measured close to the furnace by a capacitive pressure gauge (MKS 626B Baratron). For plasma processing, we supply 130 sccm of hydrogen (99.9999% purity), at a pressure of ~400 mTorr, dissipating 20 W in the plasma discharge. Our vacuum system is regularly tested for air leaks, with a detection limit ~10^{-9} mbar L/sec, to exclude the possibility that oxygen species lead to the etch phenomena reported here.

Residual hydrocarbon polymers deposited by the exfoliation process could potentially induce, prevent, or participate in reactions of hydrogen plasma with graphene sheets. To remove these unavoidable organic contaminants, samples are thermally pretreated in partial oxygen atmosphere at 500 °C for 1–2 h immediately prior to hydrogen plasma exposure. This cleaning step uses a mixture of 500 sccm argon (99.999% purity) and 50 sccm oxygen (99.993% purity), at a total pressure of 1 atm.[57]

The oxidative cleaning step does not influence the phenomena induced by hydrogen plasma exposure, as seen from the following control experiments. Supporting Information, Figure S7 shows AFM and Raman scans of a graphene/SiO_2 sample that has been exposed to Ar/O_2 atmosphere at 500 °C for 1 h, without subsequent hydrogen plasma treatment. The absence of etch features in AFM images, in monolayer and multilayer sheets alike, and the observation that the Raman D-band is not enhanced by the oxidative cleaning step, indicate that our oxidative pretreatment is mild enough that it removes organic contaminants but does not etch graphene or induce defects, to the detection limits of our AFM and Raman measurements. (At oxygen partial pressures significantly higher than ours, the etching of graphene during thermal treatment has been reported.[19,50])

Conversely, Supporting Information, Figure S8 shows Raman and AFM images of a sample after exposure to hydrogen plasma at 500 °C for 10 min, without performing an oxidative pretreatment. The only noticeable effect of omitting the oxidative cleaning step is a greater degree of particle contamination, presumably formed from hydrocarbon polymers while the sample was at elevated temperature and/or exposed to hydrogen plasma. Other than this, the same phenomena are apparent in this control sample as in samples treated with our regular procedure. Monolayer graphene sheets exhibit circular etch pits, while bilayer and thicker graphene sheets do not appear etched, with the exception of a few anisotropic etch pits, similar to those shown in Figure 4.

Muscovite mica sheets (SPI Supplies, grade V-1, P/N 01868-CA) are cleaved with adhesive tape in ambient atmosphere.

Immediately before graphene exfoliation and after cleavage, the mica sheets are heated at 200 °C on a hot plate for 10 min in ambient air. Graphene sheet thicknesses on mica are identified, similarly to graphene on SiO_2, with a combination of optical microscopy contrast, Raman spectroscopy and AFM imaging.

Tapping mode AFM images are acquired at ambient on a Park XE-100 microscope, using cantilevers with a nominal spring constant of 40 N/m (Applied NanoStructures, ACTA cantilevers). Raman measurements are performed on a WiTec alpha500 confocal scanning Raman microscope, with an excitation laser of 532 nm wavelength and a 100× objective. Spatial resolution is diffraction-limited, with a laser spot size ~0.4 μm. The total incident laser power is kept at 1−3 mW to avoid heating effects and damage to the sample. For Raman spectral mapping, scans are performed with integration times of 0.2−1 s/pixel.

Conflict of Interest: The authors declare no competing financial interest.

Acknowledgment. The authors thank Z. Bao, A. Garcia, J. McVittie, and R. Zare for technical assistance and helpful discussions. G.D. was supported by a Stanford Graduate Fellowship; M.N. was sponsored by the Department of the Navy, Office of Naval Research MURI on graphene. Construction of the furnace was supported by the Center on Nanostructuring for Efficient Energy Conversion (CNEEC) at Stanford University, an Energy Frontier Research Center funded by the U.S. Department of Energy, Office of Science, Office of Basic Energy Sciences under Award Number DE-SC0001060. We acknowledge the use of equipment in the Stanford Nanofabrication Facility (a member of the National Nanotechnology Infrastructure Network) supported by the NSF under Grant ECS-9731293, as well as the Stanford Nanocharacterization Laboratory.

Supporting Information Available: Experimental setup diagram. Further examples of the reaction of monolayer graphene with hydrogen plasma at 500 °C; localization of the Raman D-band on the edges of etch pits and sheets; evidence of the involvement of the SiO_2 substrate in the reaction. Discussion of the time-dependence of the etch rate in monolayers. Discussion of p-type doping and the lack of hydrogenation in graphene samples after hydrogen plasma exposure, and of graphene deposited on mica substrates. Data from control experiments demonstrating that the thermal cleaning step used before plasma treatment does not influence the reaction. This material is available free of charge *via* the Internet at http://pubs.acs.org.

REFERENCES AND NOTES

1. Castro Neto, A. H.; Guinea, F.; Peres, N. M. R.; Novoselov, K. S.; Geim, A. K. The Electronic Properties of Graphene. *Rev. Mod. Phys.* **2009**, *81*, 109–162.
2. Avouris, P. Graphene: Electronic and Photonic Properties and Devices. *Nano Lett.* **2010**, *10*, 4285–4294.
3. Schwierz, F. Graphene Transistors. *Nat. Nanotechnol.* **2010**, *5*, 487–496.
4. Cheng, S.-H.; Zou, K.; Okino, F.; Gutierrez, H. R.; Gupta, A.; Shen, N.; Eklund, P. C.; Sofo, J. O.; Zhu, J. Reversible Fluorination of Graphene: Evidence of a Two-Dimensional Wide Bandgap Semiconductor. *Phys. Rev. B* **2010**, *81*, 205435.
5. Balog, R.; Jørgensen, B.; Wells, J.; Laegsgaard, E.; Hofmann, P.; Besenbacher, F.; Hornekaer, L. Atomic Hydrogen Adsorbate Structures on Graphene. *J. Am. Chem. Soc.* **2009**, *131*, 8744–8745.
6. Wehling, T. O.; Novoselov, K. S.; Morozov, S. V.; Vdovin, E. E.; Katsnelson, M. I.; Geim, A. K.; Lichtenstein, A. I. Molecular Doping of Graphene. *Nano Lett.* **2008**, *8*, 173–177.
7. Nistor, R. A.; Newns, D. M.; Martyna, G. J. The Role of Chemistry in Graphene Doping for Carbon-Based Electronics. *ACS Nano* **2011**, *5*, 3096–3103.
8. Zhou, G.; Wang, D.-W.; Yin, L.-C.; Li, N.; Li, F.; Cheng, H.-M. Oxygen Bridges between NiO Nanosheets and Graphene for Improvement of Lithium Storage. *ACS Nano* **2012**, *6*, 3214–3223.
9. Loh, K. P.; Bao, Q.; Eda, G.; Chhowalla, M. Graphene Oxide as a Chemically Tunable Platform for Optical Applications. *Nat. Chem.* **2010**, *2*, 1015–1024.
10. Sun, Y.; Wu, Q.; Shi, G. Graphene Based New Energy Materials. *Energy Environ. Sci.* **2011**, *4*, 1113–1132.
11. Shao, Y.; Wang, J.; Wu, H.; Liu, J.; Aksay, I.; Lin, Y. Graphene Based Electrochemical Sensors and Biosensors: A Review. *Electroanalysis* **2010**, *22*, 1027–1036.
12. Li, C.; Adamcik, J.; Mezzenga, R. Biodegradable Nanocomposites of Amyloid Fibrils and Graphene with Shape-Memory and Enzyme-Sensing Properties. *Nat. Nanotechnol.* **2012**, *7*, 421–427.
13. Miao, X.; Tongay, S.; Petterson, M. K.; Berke, K.; Rinzler, A. G.; Appleton, B. R.; Hebard, A. F. High Efficiency Graphene Solar Cells by Chemical Doping. *Nano Lett.* **2012**, *12*, 2745–2750.
14. Sharma, R.; Baik, J. H.; Perera, C. J.; Strano, M. S. Anomalously Large Reactivity of Single Graphene Layers and Edges toward Electron Transfer Chemistries. *Nano Lett.* **2010**, *10*, 398–405.
15. Koehler, F. M.; Jacobsen, A.; Ensslin, K.; Stampfer, C.; Stark, W. J. Selective Chemical Modification of Graphene Surfaces: Distinction between Single- and Bilayer Graphene. *Small* **2010**, *6*, 1125–1130.
16. Li, W.; Tan, C.; Lowe, M. A.; Abruña, H. D.; Ralph, D. C. Electrochemistry of Individual Monolayer Graphene Sheets. *ACS Nano* **2011**, *5*, 2264–2270.
17. Ryu, S.; Han, M. Y.; Maultzsch, J.; Heinz, T. F.; Kim, P.; Steigerwald, M. L.; Brus, L. E. Reversible Basal Plane Hydrogenation of Graphene. *Nano Lett.* **2008**, *8*, 4597–4602.
18. Ryu, S.; Liu, L.; Berciaud, S.; Yu, Y.-J.; Liu, H.; Kim, P.; Flynn, G. W.; Brus, L. E. Atmospheric Oxygen Binding and Hole Doping in Deformed Graphene on a SiO_2 Substrate. *Nano Lett.* **2010**, *10*, 4944–4951.
19. Liu, L.; Ryu, S.; Tomasik, M. R.; Stolyarova, E.; Jung, N.; Hybertsen, M. S.; Steigerwald, M. L.; Brus, L. E.; Flynn, G. W. Graphene Oxidation: Thickness-Dependent Etching and Strong Chemical Doping. *Nano Lett.* **2008**, *8*, 1965–1970.
20. Gokus, T.; Nair, R. R.; Bonetti, A.; Böhmler, M.; Lombardo, A.; Novoselov, K. S.; Geim, A. K.; Ferrari, A. C.; Hartschuh, A. Making Graphene Luminescent by Oxygen Plasma Treatment. *ACS Nano* **2009**, *3*, 3963–3968.
21. Lin, Y.-C.; Lin, C.-Y.; Chiu, P.-W. Controllable Graphene N-doping with Ammonia Plasma. *Appl. Phys. Lett.* **2010**, *96*, 133110.
22. Elias, D. C.; Nair, R. R.; Mohiuddin, T. M. G.; Morozov, S. V.; Blake, P.; Halsall, M. P.; Ferrari, A. C.; Boukhvalov, D. W.; Katsnelson, M. I.; Geim, A. K.; Novoselov, K. S. Control of Graphene's Properties by Reversible Hydrogenation: Evidence for Graphane. *Science* **2009**, *323*, 610–613.
23. Han, M. Y.; Brant, J. C.; Kim, P. Electron Transport in Disordered Graphene Nanoribbons. *Phys. Rev. Lett.* **2010**, *104*, 056801.
24. Todd, K.; Chou, H.-T.; Amasha, S.; Goldhaber-Gordon, D. Quantum Dot Behavior in Graphene Nanoconstrictions. *Nano Lett.* **2009**, *9*, 416–421.
25. Lakshmi, S.; Roche, S.; Cuniberti, G. Spin-Valve Effect in Zigzag Graphene Nanoribbons by Defect Engineering. *Phys. Rev. B* **2009**, *80*, 193404.
26. Luo, Z.; Yu, T.; Kim, K.-J.; Ni, Z.; You, Y.; Lim, S.; Shen, Z.; Wang, S.; Lin, J. Thickness-Dependent Reversible Hydrogenation of Graphene Layers. *ACS Nano* **2009**, *3*, 1781–1788.
27. Yang, R.; Zhang, L.; Wang, Y.; Shi, Z.; Shi, D.; Gao, H.; Wang, E.; Zhang, G. An Anisotropic Etching Effect in the Graphene Basal Plane. *Adv. Mater.* **2010**, *22*, 4014–4019.
28. Shi, Z.; Yang, R.; Zhang, L.; Wang, Y.; Liu, D.; Shi, D.; Wang, E.; Zhang, G. Patterning Graphene with Zigzag Edges by Self-Aligned Anisotropic Etching. *Adv. Mater.* **2011**, *23*, 3061–3065.
29. Novoselov, K.; Geim, A.; Morozov, S.; Jiang, D.; Y., Z.; Dubonos, S.; Grigorieva, I.; Firsov, A. Electric Field Effect in Atomically Thin Carbon Films. *Science* **2004**, *306*, 666–669.
30. Ferrari, A.; Meyer, J.; Scardaci, V.; Casiraghi, C.; Lazzeri, M.; Mauri, F.; Piscanec, S.; Jiang, D.; Novoselov, K.; Roth, S.; Geim, A. Raman Spectrum of Graphene and Graphene Layers. *Phys. Rev. Lett.* **2006**, *97*, 187401.

31. Nemes-Incze, P.; Magda, G.; Kamarás, K.; Biró, L. P. Crystallographic Orientation Dependent Etching of Graphene Layers. *Phys. Stat. Sol. C* **2010**, *7*, 1241–1245.
32. Chang, H.; Bard, A. J. Formation of Monolayer Pits of Controlled Nanometer Size on Highly Oriented Pyrolytic Graphite by Gasification Reactions as Studied by Scanning Tunneling Microscopy. *J. Am. Chem. Soc.* **1990**, *112*, 4598–4599.
33. Chang, H.; Bard, A. J. Scanning Tunneling Microscopy Studies of Carbon-Oxygen Reactions on Highly Oriented Pyrolytic Graphite. *J. Am. Chem. Soc.* **1991**, *113*, 5588–5596.
34. McCarroll, B.; McKee, D. The Reactivity of Graphite Surfaces with Atoms and Molecules of Hydrogen, Oxygen and Nitrogen. *Carbon* **1971**, *9*, 301–311.
35. Nunomura, S.; Kondo, M. Characterization of High-Pressure Capacitively Coupled Hydrogen Plasmas. *J. Appl. Phys.* **2007**, *102*, 093306.
36. Yamada, Y.; Yamada, T.; Tasaka, S.; Inagaki, N. Surface Modification of Poly(tetrafluoroethylene) by Remote Hydrogen Plasma. *Macromolecules* **1996**, *29*, 4331–4339.
37. Mendez, I.; Gordillo-Vazquez, F. J.; Herrero, V. J.; Tanarro, I. Atom and Ion Chemistry in Low Pressure Hydrogen DC Plasmas. *J. Phys. Chem. A* **2006**, *110*, 6060–6066.
38. Roth, J.; Garcia-Vazquez, C. Analytic Description of the Chemical Erosion of Graphite by Hydrogen Ions. *Nucl. Fusion* **1996**, *36*, 1647–1659.
39. Mech, B. V.; Haasz, A. A.; Davis, J. W. Model for the Chemical Erosion of Graphite Due to Low-Energy H^+ and D^+ Impact. *J. Appl. Phys.* **1998**, *84*, 1655–1669.
40. Liu, S.; Sun, J.; Dai, S.; Stirner, T.; Wang, D. A General Model for Chemical Erosion of Carbon Materials Due to Low-Energy H^+ Impact. *J. Appl. Phys.* **2010**, *108*, 073302.
41. Rosner, D. E. High-Temperature Gas−Solid Reactions. *Annu. Rev. Mater. Sci.* **1972**, *2*, 573–606.
42. Wood, B. J.; Wise, H. Reaction Kinetics of Gaseous Hydrogen Atoms with Graphite. *J. Phys. Chem.* **1969**, *73*, 1348–1351.
43. Wood, B. J.; Wise, H. Kinetics of Hydrogen Atom Recombination on Surfaces. *J. Phys. Chem.* **1961**, *65*, 1976–1983.
44. Boukhvalov, D. W.; Katsnelson, M. I. Enhancement of Chemical Activity in Corrugated Graphene. *J. Phys. Chem. C* **2009**, *113*, 14176–14178.
45. Cullen, W. G.; Yamamoto, M.; Burson, K. M.; Chen, J. H.; Jang, C.; Li, L.; Fuhrer, M. S.; Williams, E. D. High-Fidelity Conformation of Graphene to SiO_2 Topographic Features. *Phys. Rev. Lett.* **2010**, *105*, 215504.
46. Ishigami, M.; Chen, J. H.; Cullen, W. G.; Fuhrer, M. S.; Williams, E. D. Atomic Structure of Graphene on SiO_2. *Nano Lett.* **2007**, *7*, 1643–1648.
47. Bahr, J. L.; Tour, J. M. Covalent Chemistry of Single-Wall Carbon Nanotubes. *J. Mater. Chem.* **2002**, *12*, 1952–1958.
48. Lui, C. H.; Liu, L.; Mak, K. F.; Flynn, G. W.; Heinz, T. F. Ultraflat Graphene. *Nature* **2009**, *462*, 339–341.
49. Xu, K.; Cao, P.; Heath, J. R. Graphene Visualizes the First Water Adlayers on Mica at Ambient Conditions. *Science* **2010**, *329*, 1188–1191.
50. Yamamoto, M.; Einstein, T. L.; Fuhrer, M. S.; Cullen, W. G. Charge Inhomogeneity Determines Oxidative Reactivity of Graphene on Substrates. *ACS Nano* **2012**, *6*, 8335–8341.
51. Wang, Q. H.; Jin, Z.; Kim, K. K.; Hilmer, A. J.; Paulus, G. L.; Shih, C.-J.; Ham, M.-H.; Sanchez-Yamagishi, J. D.; Watanabe, K.; Taniguchi, T.; *et al.* Understanding and Controlling the Substrate Effect on Graphene Electron-Transfer Chemistry *via* Reactivity Imprint Lithography. *Nat. Chem.* **2012**, *4*, 724–732.
52. Zhang, Y.; Brar, V. W.; Girit, C.; Zettl, A.; Crommie, M. F. Origin of Spatial Charge Inhomogeneity in Graphene. *Nat. Phys.* **2009**, *5*, 722–726.
53. Tan, Y.-W.; Zhang, Y.; Bolotin, K.; Zhao, Y.; Adam, S.; Hwang, E. H.; Das Sarma, S.; Stormer, H. L.; Kim, P. Measurement of Scattering Rate and Minimum Conductivity in Graphene. *Phys. Rev. Lett.* **2007**, *99*, 246803.
54. Müller, K.; Chang, C. Electric Dipoles on Clean Mica Surfaces. *Surf. Sci.* **1969**, *14*, 39–51.
55. Ni, Z. H.; Wang, H. M.; Luo, Z. Q.; Wang, Y. Y.; Yu, T.; Wu, Y. H.; Shen, Z. X. The Effect of Vacuum Annealing on Graphene. *J. Raman Spectrosc.* **2009**, *41*, 479–483.
56. Dean, C. R.; Young, A. F.; Meric, I.; Lee, C.; Wang, L.; Sorgenfrei, S.; Watanabe, K.; Taniguchi, T.; Kim, P.; Shepard, K. L.; Hone, J. Boron Nitride Substrates for High-Quality Graphene Electronics. *Nat. Nanotechnol.* **2010**, *5*, 722–726.
57. Garcia, A. G. F.; Neumann, M.; Amet, F.; Williams, J. R.; Watanabe, K.; Taniguchi, T.; Goldhaber-Gordon, D. Effective Cleaning of Hexagonal Boron Nitride for Graphene Devices. *Nano Lett.* **2012**, *12*, 4449–4454.